Coordination Chemistry Reviews 255 (2011) 1970–1980

Contents lists available at ScienceDirect

Coordination Chemistry Reviews

journal homepage: www.elsevier.com/locate/ccr

Review

Molecular scale bioelectrochemistry

A.V. Patil, J.J. Davis*

Department of Chemistry, University of Oxford, Physical and Theoretical Teaching Laboratory, South Parks Road, Oxford, Oxfordshire OX1 3QZ, UK

Contents

ARTICLE INFO

Article history:
Received 8 December 2010
Received in revised form 28 January 2011
Accepted 2 February 2011
Available online 9 February 2011

Keywords:
Molecular
Electrochemistry
Azurin
Tunnelling
Fluorescence
Voltammetry

ABSTRACT

Our ability to interface with biological macromolecules continues to advance at a significant pace and brings with it potential applications that are as broad as they are powerful. Running alongside this evolution has been the refinement of methods by which interfaces can be probed at scales approaching (or being at) the molecular. Through combinations of experimental design, proximal probe technology and high sensitivity optical imaging, one can truly probe the bioelectronic interface at levels that are both startling and associated with unprecedented levels of detail.

1. Introduction

Redox active proteins and enzymes are integral in the fundamental biological energy transduction processes which sustain life. The electrochemical interrogation of such moieties leads to an enhanced understanding of natural molecular evolution and the structural features which confer desired properties (enabling, for example, designed engineering by site directed mutagenesis), and directly requires that effective methods are developed which enable communication at man-made interfaces (electrodes). In a significant number of specific cases, the latter has been pivotal in not only decoding kinetic and thermodynamic aspects of intramolecular and interfacial (heterogeneous) electron transfer but also in the generation of enzyme based biosensors. We briefly review here the fundamental concepts of practical (bulk) bioelectrochemistry and the application of techniques which allow controlled non-destructive surface assembly and electronic interfacing. The core part of this review will be associated with a detailing of efforts to move these inherently grossly averaging electrochemical analyses to a more refined molecular scale and, within this, two methodologies; the first is the application of near field scanning probe methods to both visualizing and then directly probing redox characteristics of single molecules (gated single molecule conductance). The second is the development and application of interfacial fluorescence-detected cyclic voltammetry (FCV), a far field optical means of directly imaging and spatially resolving kinetic and thermodynamic electron transfer characteristics within a population of surface confined biomolecules.

2. Controlled assembly & interfacing

The road to controlled bioelectronic interfacing started more than three decades ago with pioneering reports of reversible diffusion controlled direct electron transfer of the respiratory heme

* Corresponding author. Tel.: +44 1865 275914; fax: +44 1865 275410.
E-mail address: Jason.davis@chem.ox.ac.uk (J.J. Davis).

0010-8545/$ – see front matter © 2011 Elsevier B.V. All rights reserved.
doi:10.1016/j.ccr.2011.02.002

protein cytochrome *c* at suitably modified gold or indium tin oxide electrodes [1,2]. Since then a variety of surface modifications, ranging from self assembled monolayers (SAMs), nanoparticle modified surfaces to sol gels, have been utilized in mediating electron transfer with a library of metalloproteins and enzymes [3–7].

The advantages of confining the bioelectrochemical system to the electrode surface can be considerable if this can be achieved non-destructively; the amount of material required reduces/diminishes by several orders of magnitude, the potentially distorting contributions of sluggish diffusion vanish, data (particularly kinetic) are thereby more easily interpreted, and surface spectroscopic/imaging tools can be powerfully applied. The surfaces employed in these analyses are, now, highly varied both topographically and chemically. They include not only interfaces based on modifications of the noble metal, carbon or metal oxide electrodes which are well known in electroanalysis but also those which are deliberately "nanostructured" or based on polymer modifications.

In sol–gel immobilization, for example, a silicate matrix is formed by the hydrolysis of an alkoxide precursor, typically tetraethyl orthosilicate, followed by condensation to yield a network of siloxanes. The addition of a protein after partial hydrolysis (before full gelation) leads to its entrapment within a porous aqueous microenvironment. The modifications are typically applied to an electrode surface before complete gelation by dip coating. The resulting films have been found to be chemically, thermally and structurally stable and capable of sustaining a high degree of biofunctionality [8–13]. Another approach, and one which has found extensive biosensor application, is bioimmobilization in or on electrogenerated polymer films where the molecule is either physically entrapped within the polymer matrix or covalently bonded to it. This methodology benefits from the high levels of control and reproducibility associated with the film generation [14].

Carbon nanotubes (CNTs), coaxial cylindrical graphite sheets of nanometre diameter, uniquely combine conductance, chemical stability and mechanical characteristics which are of considerable potential application electrochemically. Multiwall carbon nanotubes (MWNT) films were first used by Davis and Hill in the realisation of direct protein electrochemistry [15–17]. Since then, CNT modified surfaces have been applied to the bioelectrochemical interrogation of a number of proteins and enzymes [18–21]. Most notable amongst recent work have been reports by the group of Rusling in exploiting enzymes covalently attached to the end of vertically oriented single-wall carbon nanotube "forest" arrays [22–24]. Other nanostructured interfaces such as those generated from Au colloids or metal oxide nanoparticles have also been productively applied in enzyme voltammetry [5,25–31].

A vast amount of bioelectrochemical literature now exists at the planar electrode surfaces presented by as-prepared or chemically modified ITO [32,33], silicon[34,35], diamond [36] and pyrolytic carbon [37–41]. Alkanethiol SAM modified noble metal surfaces probably remain, though, the most defined, chemically tuneable, and spectroscopically characterisable interfaces on which to analyze biomolecular electron transfer [42].

Cytochrome *c* and azurin represent the two most well studied surface assembled biomolecular systems in this context. The former is a small heme protein involved in mitochondrial respiration and adsorbs strongly at ω-mercaptocarboxylic acid SAMs by virtue of favourable electrostatic interactions with a patch of cationic lysine residues close to the heme solvent exposed edge [43–47]. Azurin (shown in Fig. 1), is a blue copper protein found in the respiratory chain of denitrifying bacteria. It possesses a hydrophobic surface region that plays important role in electron transfer and binding [48–50]. Films of the protein on thiol SAMs have been characterized at molecular scales by others and us by SERS, electroreflectance and an extensive barrage of voltammetric methods [3,51–57]. Orientational control of this protein on methyl terminating thiol adlayers has been confirmed in experiments where the electron transfer kinetics to underlying gold electrode surfaces have been mapped and modulated across a range of film thicknesses [3,58,59]. The predominance of hydrophobic forces in this protein-surface association has also been confirmed and energetically estimated [3,51].

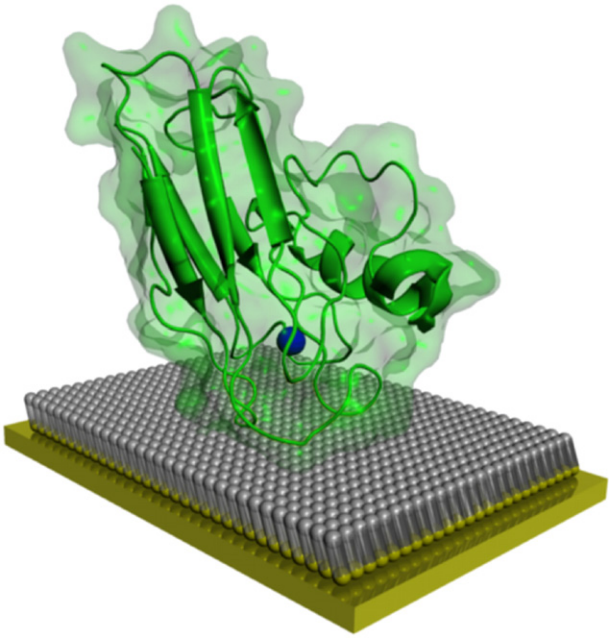

Fig. 1. Cartoon representation of azurin (adapted from PDB 1AZU [145]) physisorbed on a methyl-terminated self assembled monolayer through a hydrophobic patch which orients the molecule so as to bring the copper redox centre (blue sphere) into efficient electronic coupling with the supporting gold electrode surface.

The effectiveness of an oriented surface immobilization in maximizing electronic coupling to an underlying electrode while minimizing the dispersion and experiment-to-experiment variance inherent in less ordered biomolecular films is obvious. Another approach is the utilization of site directed mutagenesis, and, in particular, the site specific introduction of anchoring cysteine or HIS tag residues into a proteins solvent exposed surface. The former can be used to anchor proteins and enzymes on either pristine bare gold electrodes or suitably SAM modified surfaces [60–64]. Such an "engineered" oriented protein adlayer facilitates investigations of molecular chemisorption, orientational effects on electron transfer and enzymatic activity, and direct (topographic and tunnelling) imaging at truly molecular levels [54,61,65–68].

3. Molecular level electrochemistry; accessing hidden information

Though the surface confinement of biomolecules of interest on carefully engineered/modified electrode surfaces enables a potentially powerful range of voltammetric and spectroscopic analyses to be applied, in all cases the acquired data are averaged over a very large number of molecules (typically 10^{11}–10^{14}; depending upon the surface coverage and electrode area). This then means that the "bulk" measurement is of a weighted average property distribution rather than a mapping of this distribution itself. With this inherent limitation it is significant to note that all classical electrochemical theories of faradaic electron transfer commence with an assumption of interfacial (and molecular) homogeneity. Observed "non ideal" electrochemical responses are ubiquitous, however, and have been loosely ascribed to kinetic and thermodynamic dispersion across supporting surfaces, something that is expected

to depend upon degree of electrode surface pre-treatment, the combined effects of lateral molecular interaction, structural perturbations of the redox active entity, variations in surface charge, molecular orientation, local dielectric constant and redox site-electrode electronic coupling. These effects and others undoubtedly also contribute to experiment to experiment variation (even with chemically simple and robust redox species, current and peak separation deviations of up to 10% are common). A number of published reports have ascribed the inhomogeneity in electrochemical response attained from an array of surface confined redox active proteins to a distribution of potential with the electrode double layer [69,70]. Clark et al. have specifically proposed, for example, that a distribution in formal potential arises from subpopulations of adsorbed proteins molecules each localized in a different interfacial microenvironment [71]. Nahir et al. have assigned the distribution of electron transfer rate constants to an associated distribution in distance between the redox centres and underlying electrode [44]. The group of Bowden have reported influences of protein surface charge on subsequently observed electron transfer thermodynamics and additionally considered charge-transfer induced alterations of interfacial potential distribution [72]. Recently the group of Bard have reported a direct optical observation of thermodynamic dispersion in the (largely irreversible) voltammetry of polymeric nanoparticles spun onto ITO surfaces [73,74].

While the topographical heterogeneity of the electrode surface is readily mapped by scanning probe experiments, a clear prediction of the impact this will have on observed voltammetry is still lacking. A detailed appreciation of heterogeneity remains, therefore, a subject in need of investigation and a pre-requisite if a truly molecular level of understanding of metalloproteins voltammetry is to be achieved or derived molecular scale bioelectronic devices to be, in any way, predictable.

Bard et al. have previously demonstrated the amplified redox analysis of a single redox molecule trapped within the confines of a scanning electrochemical junction in solution [75,76]. More practically (these experiments can neither directly resolve interfacial electron transfer energetics nor can be readily extended to investigation of bioelectrochemical systems), one may seek to reduce the sample population by reducing the electroactive working area. Hoeben et al, for example, have resolved catalytic current responses from less than 50 enzyme molecules immobilized on lithographically fabricated nanoelectrodes [77]. Data analysis in such cases is critically dependent upon precise knowledge of electrode geometry; as electrodes fall below the micron scale reproducible fabrication and robust characterization is, though, problematic. Even with highly specialised nanoelectronic configurations, amperometric detection methodologies are limited (at best) to the femtoampere range, or some >6000 electrons per second, a sensitivity which demands a great deal of a bioelectrochemical system [77,78].

3.1. Near field analysis

Rapid technological advances in near field analysis, particularly Scanning Probe Microscopy (SPM), have brought about an unprecedented ability to visualize molecular films and even individual molecules confined to an electrode surface. SPM, in which the varied interactions between a probe and sample of interest are mapped as a specific probe is raster scanned, has emerged as a key tool for molecular imaging of biological samples as it can provide high-resolution images which are comparable to those of electron microscopy with the additional advantage that the sample can be imaged under a flexible environment that can closely mimic physiological (typically a buffer at appropriate pH). The ability to "touch" the sample has opened up multiple avenues of investigation which have now progressed beyond observations of topography to include the quantification of recognition forces, biological fold analysis, single protein/molecule manipulation, and conductance/electron transfer analyses [79–87].

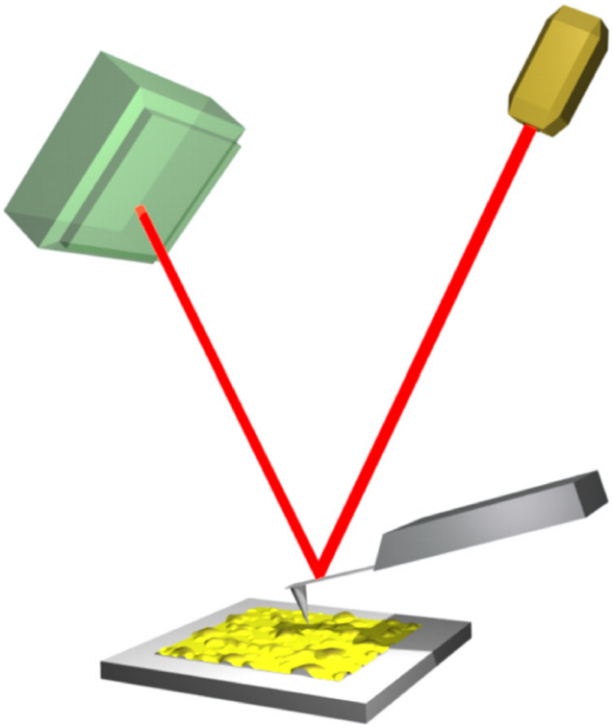

Fig. 2. Schematic representation of an AFM configuration (not to scale) showing a soft (low spring constant) cantilever with a sharp probing tip that is scanned with a piezoscanner (not shown) over a sample with subnanometer scale accuracy while its deflections are mapped by the positional modulations of a reflected laser beam on a split photodiode (green). The photodiode response is interpreted by appropriate software, pixel-by-pixel, and enables a truly three dimensional surface mapping with nanometre resolution.

In Atomic Force Microscopy (AFM), the most frequently used SPM configuration, the probe is a sharp microfabricated silicon/silicon nitride tip (with a radius typically between 10 and 20 nm) attached at the terminus of a flexible cantilever a few hundred microns in size. The interactions between the probe and the underlying sample (the latter normally mounted on a piezoelectric scanner (with movement in horizontal and vertical direction), are mapped by the bending of the cantilever, itself monitored by an optical lever configuration i.e., variations in the position of reflected laser beam as monitored by a split photodiode (Fig. 2). With soft cantilevers it is possible to sense interaction forces as low as few picoNewtons; modern piezoelectric scanners can translate the sample or tip in the x, y and z direction with sub-nanometre resolution thus giving AFM a capacity to both render 3D images of the (surface or surface-confined) sample with atomic resolution and the ability to manipulate at the molecular level [84,88,89].

AFM imaging can be sub-classified according to the modes of tip–sample interaction; in contact mode the probe is in perpetual contact with the sample while in "tapping mode" it is oscillating (near its resonant frequency) and in contact with the surface only transiently at the lower extreme of its oscillation. While it is possible to achieve high resolution biological imaging in contact mode, most notably with membrane protein crystals [90,91] and DNA [92,93], destructive tip–sample interactions can be difficult to avoid with soft or compressible samples, even those which are rigidly confined, leading to image deformation and artefacts. In "tapping mode", lateral ("dragging") forces imparted on the sample are dramatically reduced by limiting interactions to a periodic "tapping". The energy dissipation between the driven probe and surface at

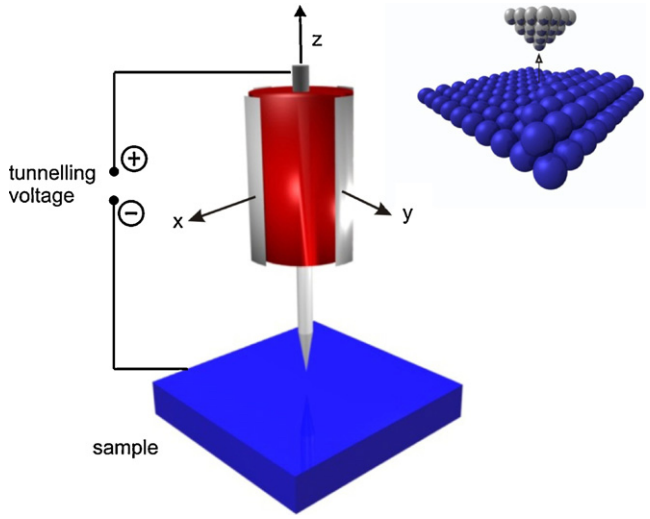

Fig. 3. Schematic of Scanning Tunnelling Microscope (not to scale). When a piezoelectric tube (red) scans a sharp metallic tip over a conductive sample (blue) with the application of a moderate voltage bias, electrons quantum mechanically tunnel across the gap to produce a (pico to nano ampere) current. Inset: tunnelling current is exquisitely sensitive to structure at or within the junction. For a suitably sharpened tip (ideally, one that terminates in a single atom) this current is confined laterally to a radius of sub-angstrom proportions. The remarkable spatial resolution of the STM derives from this lateral current confinement. By detecting the very fine changes in current pixel by pixel a two-dimensional map of the corrugations in electron density of the surface is obtained.

contact leads to a change in amplitude which serves as the feedback signal in topographic image generation. Changes in the oscillation phase can additionally be measured and related to surface adhesion, friction and sample viscoelastic properties [94,95]. In another variation of tip–sample interaction, Chemical Force Microscopy (CFM) employs a functionalized AFM probe to map changes in torsional force (friction) on the probe and, in so doing, can chemically map surface functionality with nanometre resolution [96,97]. These forms of imaging and others in the AFM armoury have been successfully applied to the nanometre or even sub-nanometre resolution topographic imaging of electrode surface confined proteins under a variety of highly controllable conditions [98–102].

In Scanning Tunnelling Microscopy (STM) analyses of surface confined proteins, a small voltage is applied between the proximal probe (typically an ultra-sharp metallic tip fabricated by electrochemical etching) and underlying pristine electrode in an ultraclean environment. The probe is then bought into increasingly close approach to the (usually planar) electrode by feedback electronics and motors until the tunnelling of electrons commences (Fig. 3). The measured current has an inversely exponential relationship with the probe–substrate separation distance and is recorded pixel by pixel as these two interfaces scan relative to each other. Alternatively, the tunnelling current can be used as a feedback loop in order to actuate the probe or underlying substrate. In either mode, spatial resolutions are routinely on atomic scale (it is worth noting that STM does not map out true topography of the sample rather a surface of constant tunnelling probability). Within the tunnel current mapping, modern electronics are capable of measuring on the femtoampere scale enabling surface feature detection on the tenths of an ångström scale. Lateral resolution is limited by the probe geometry, most notably the radius of curvature, and the mechanical and immobilization characteristics of the sample but is typically on the angstrom to low nanometre scale with surface confined molecules. In general, on account of the lower tip contact area and sensitivity of current on separation and intervening electronic structure, STM methods offer an inherently higher resolution than AFM. Moreover, since imaging directly involves the mapping out of interactions between electrons and surface immobilized molecules, a good deal of information on molecular conductance and electronic structure can be acquired [103–105]. Significantly, from the context of this article, the requirement of a measurable current flow does not preclude the imaging of (classically insulating) biological macromolecules. Unlike AFM however, STM systems are, therefore, most effectively applied to atomic and molecular-scale analysis and are unsuitable for the characterisation of larger entities such as live cells. It is additionally worth noting that the applied bias in an STM experiment is dropped entirely across the small tip–substrate gap resulting in an immense electric field gradient (typically exceeding 100 MV m^{-1}). The role this field may have in changing native levels of molecular solvation or (related) re-organisational energies remains significant although rather poorly defined [106].

The controlled interfacing of metalloproteins and enzymes with electrodes, including both the direct anchoring of protein to metallic surfaces, the physical sorption of protein on carbonaceous electrodes and the immobilization on SAM modified surfaces, is now routinely mapped by both AFM and STM [3,101,107–112]. The immobilization of engineered azurin molecules on gold electrodes through site specifically introduced surface cysteine residues has, for example, been verified and followed in real time by AFM and STM [60,65]. Similar studies with poplar plastocyanin mutants absorbed on gold, by either a disulfide bridge or a single thiol, have demonstrated that dimensions as evaluated by SPM can lie well within the range predicated by crystallographic studies [113]. Such studies, more generally, give an insight into the kinetics of protein-electrode association, film stability and protein film homogeneity. During the past decade, developments in the ability of proximal probes to analyze molecular systems with a nanometre spatial resolution has evolved progressively away from "just" imaging to a more functional analysis (mechanical assessments, electrostatic measurements, conductance assays etc.).

3.2. Bio(molecular) electronic and redox linked conductance

Though undoubtedly very powerful from an imaging perspective, one of the significant drawbacks of the STM configuration is that there is no direct control over the force imparted on the molecular system under analysis. Such forces, and their associated electric fields, can feasibly be highly perturbative (not only in terms of mechanical structure but also in terms of, for example, the reorganizational energy associated with a redox event; see ECSTM below). Since the probe may feasibly be either partially "buried" within the molecule or sitting a number of ångströms above it, the resulting tunnelling current is a convolution of many contributions, making absolute measurements of conductance very difficult. For direct analyses of molecular conductance Conducting Atomic Force Microscopy (CP-AFM), where in an AFM tip is coated in a metallic layer and contacted with a molecule of interest under controlled load, is more appropriate. As a result of the integral force feedback, the probe position and sample conductivity are decoupled. Since molecular structure and tunnel conductance are intrinsically linked, a time-resolved analysis of the latter can facilitate an understanding of molecular level protein dynamics under conditions of quantified compressive force. Using CP-AFM it has been possible, for example, to measure molecular conductance of a number of biomolecules and the dependence of this on the probe applied compressional force [68,114–117]. Within this work, charge transfer across the biomolecule has been both explained and simulated with a modified Simmons tunnelling model (with a protein fold resembling a featureless continuum tunnelling barrier). Using conditions of low contact force (<2–3 nN) these molecules are observed to be highly insulating by virtue a lack of a reliable electrical contact at the metallic probe. Robust electrical contact is typically

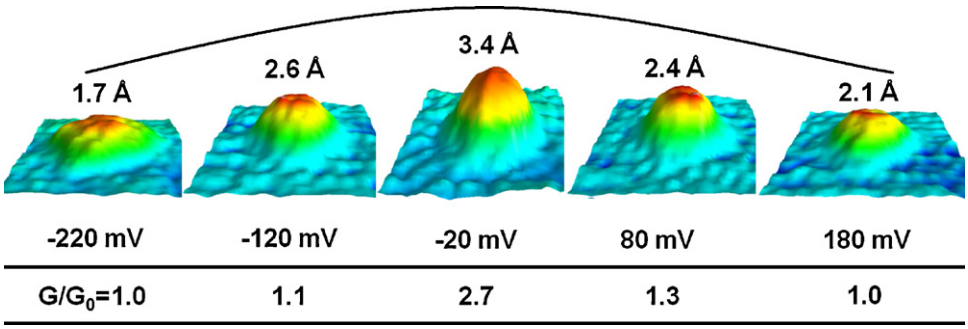

Fig. 4. 3D representation of the modulation of measured STM height of a horse heart cytochrome *c* molecule on 11-mercaptoundecanoic acid SAM as function of applied substrate potential (vs SCE). The modulation, directly equivalent to a variable molecular conductance, is attributed to the tuning of the available redox energy level relative to the Fermi energies of the two electrodes (tip and substrates). The difference between "ON" (at −0.02 V vs SCE) and "OFF" resonance (−0.22 V vs SCE; normalised G_0) measured heights of 1.7 Å corresponds to an increased conductance (G) of 2.7 fold (values here generated are averaged over 24 single molecules). Figure reproduced with permission from Ref. [53].

established at 3-10 nN of applied force at which conductance can be directly assayed (typically in the range of 30–40 GΩ [57,118]). Within obtained current–voltage curves the phenomenon of negative differential resistance (NDR) has been noted with molecules which are electrochemically active, an indication possibly indicative of resonant tunnelling through redox site orbitals [117,118].

Though probe imparted forces are unquantified, the interaction of incident electrons with redox switchable molecules is much more controllable when combining an electrochemical setup with that of an STM in a four terminal configuration under bipotentiostatic control. Within this Electrochemical STM (ECSTM), where the tunnelling tip is a working electrode, conductance analyses can be carried out under controllable conditions with simultaneous electrochemistry. The total current measured here is combination of faradaic & non-faradaic (which includes the tunnelling current and capacitative contributions) processes. In order to attenuate charging currents, it is normal to insulate all but the apex of the tunnelling electrode a procedure which becomes more demanding as ionic strengths increase and one moves solution conditions closer to those which are physiological. Under conditions of normal bias, electrons are assumed to tunnel from the tip to substrate (or in opposite direction) and not accumulate on the molecules in the gap, nor interact significantly with molecular states. Under the highly controllable conditions presented by these ECSTM configurations, however, orbital access and incident electron energy are highly tuneable parameters. These experiments, then, enable through the impact that orbital occupancy and energetic alignment have on conductance (and thus image contrast), redox processes to be directly imaged. By tuning, through imposed surface potentials, the degree to which orbital states are accessible to incident electrons, one directly tunes conductance; that is, one induces and observes transistor type conductance gating under electrolytic solution [106,119–124]. These effects have been observed with biological, as well as redox active organic moieties and inorganic complexes, despite the fact that most biomacromolecules are both formally electrically insulating and have redox active prosthetic groups which are commonly buried [115].

By the way of example, others and we have, in recent years, reported the tunnel conductance of a range of metalloproteins and enzymes [53,114,115,117,125–127]. With several of these molecular systems, it is demonstrably possible to tune the incident tunnelling energies in and out of resonance with the redox site and, in so doing, gate molecular conductance [52,57,128]. ECSTM studies of controllably oriented and electrochemically active azurin [122] or horse heart cytochrome *c* (HHCC) on bare or modified gold electrodes, form the basis of much of what has been published in terms of biomolecular systems. These molecules, in which the redox site is accessible only through the protein and (in some cases) saturated SAM dielectrics, exhibit relatively slow heterogeneous electron transfer kinetics to the underlying electrode ($\sim 10\,s^{-1}$) with a GΩ resistance. The latter is tuneable through the underlying working electrode potential across almost an order of magnitude as shown in Fig. 4. Recent theoretical and experimental analyses have suggested that a sequential two step tunnelling process is likely to be operable under such circumstances [53,106,120]. Regardless of mechanistic detail, the conductance maximum in these tunnelling junctions is typically observed at or close to the bulk determined electrochemical midpoint potential (this coincides with the point at which the redox site orbitals facilitating current flow are most energetically accessible to the supporting and probe electrodes). Since this conductance maximum can be determined for single molecules under identical tunnelling conditions one potentially has direct access not only to the electrochemical midpoint potential of single molecules but also, for the first time, the dispersion in this thermodynamic property as one maps out conductance gating across a surface population (see Fig. 5).

The interfacial information potentially provided by the application of near field proximal probes to bioelectrochemically active layers has, then, evolved progressively away from "just" molecular imaging to a more functional analysis (mechanical assessments, electrostatic measurements, conductance and redox linked conductance assays etc.). Though these assessments provide information at spatial resolutions we could only dream of a decade or two ago (molecular arrays or even individual molecules can be directly visualized on electrode surfaces and their electronic coupling/redox characteristics mapped out on a molecule-by-molecule basis), they do require in many cases, highly specialised and costly experimental configurations and a good deal of experimental skill. The application of electrochemical tunnelling imaging to the bioelectrochemical interface, in particular, does shed light intriguingly on the variance within molecular films (be it the physical distribution of molecules, molecular aggregation, or "midpoint potential"). It does, though, remain experimentally, and in the case of redox tuned conductance, also theoretically, demanding.

3.3. Optically linked electrochemistry

Several years ago we introduced, with colleagues in Leiden, Holland, the concept of directly imaging interfacial electron transfer by means of fluorescence imaging at optically transparent electrode surfaces [129]. This concept rests on the fact that, for many proteins, the redox active site is also a chromophore for which the spectral characteristics are (redox) switchable. If one binds an organic fluorophore to the periphery of such a protein, in order to establish Förster Resonance Energy Transfer (FRET) between it and the redox site, then, in principal, one can directly follow electron transfer pro-

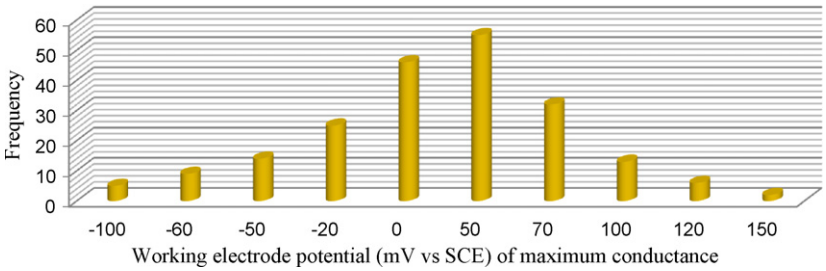

Fig. 5. In an ECSTM configuration, the incident tunnelling electrons can be tuned in and out of resonance with redox site orbital states, a process which can greatly modulate the amount of current which passes through a given molecule at a given bias (i.e. its associated conductance). The position of maximum conductance observed as one scans the potential of the supporting planar electrode lies close to the redox site midpoint potential. By plotting this potential of maximal conductance across a range of surface confined molecules, one potentially has direct access to the spread in redox properties within the population. Here data are shown for horse heart cytochrome *c* molecules immobilized on a mercaptoundecanoic acid modified gold electrode. It it noteworthy both that the maximal conductance, for most molecules, lies close to the bulk determined midpoint potential value but also spans tens of millivolts. Though the relationship between the surface potential of conductance maximum and half wave potential is subject to a number of variables, not all necessarily constant across a surface population of molecules, nearly all published works have confirmed that this coincidence is high (within a few tens of millivolts).

cesses by imaging the fluorescence emission from the appended fluorophore [130].

Initial work was carried out with fluorophore labelled azurin (Fig. 6), and has subsequently been applied to a number of blue copper proteins and enzymes [131,132]. In its oxidized state azurin displays a strong absorbance ($\varepsilon = 5.6\,mM^{-1}\,cm^{-1}$) in 550–600 nm range which corresponds to π–π^* transition centred at the copper site and involving mainly the $d_{x^2-y^2}$ orbital and a 3p orbital on the Cys112 ligand sulfur. This absorption disappears when the copper site is reduced to a d^{10} electronic configuration (Fig. 6 (inset)). This pronounced spectral change strongly modulates the fluorescent properties of a derived FRET donor–acceptor pair (Cu: acceptor, fluorophore: donor) such that in its oxidized state the metal site strongly quenches a spectrally suitable organic fluorophore while, in the reduced protein, the fluorophore is emissive [130,132].

Taking advantage of the imaging (signal: noise) refinements available in wide field Total Internal Reflection Microscopy (TIRF),

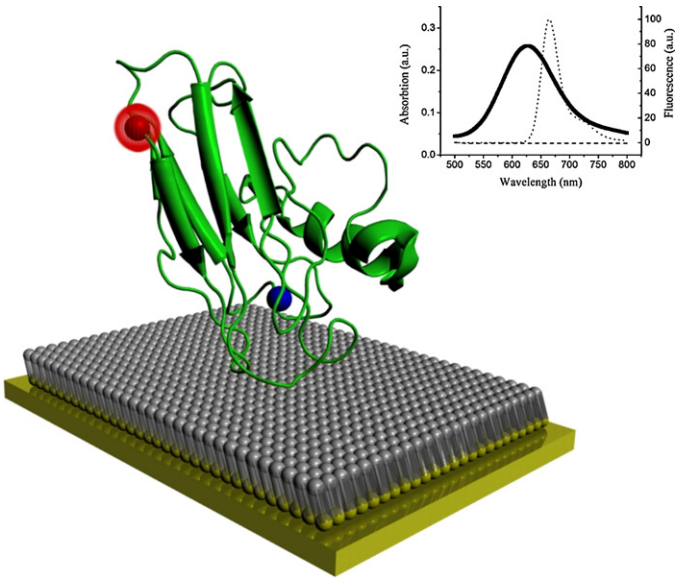

Fig. 6. Cartoon representation of *N*-terminus labelled azurin on SAM modified gold with an appended fluorophore depicted as a red sphere (the copper shown as a blue sphere). Inset: optical spectrum overlap for the azurin Cu^{2+} Cy5 FRET pair. The Cy5 emission spectrum (dotted line) was determined at excitation wavelength of 600 nm. The UV–Vis upon reduction of the metal redox centre (dashed line), eliminating the spectral overlap between the fluorophore and redox centre and turning the pathway to non-radiative energy loss from the fluorophore "off" (in effect, turning emission from the fluorophore "on"). Reproduced from Ref. [129] with permission.

where an evanescent wave is used to excite fluorophores in a restricted region of sample immediately adjacent to the surface, we have reported the application of redox coupled FRET to the direct imaging of electrochemically driven redox changes in Cy5 labelled azurin immobilized on alkyl-terminated thiol SAMs [129,133,134]. Within these experiments, a single compartment electrochemical cell containing degassed buffer and consisting of a functionalized transparent thin film gold working electrode, reference electrode and Pt gauze counter electrode is assembled on an inverted TIRF microscope (Fig. 7). Surface confined voltammetry confirms electroactive surface coverages to be $\sim 5 \times 10^{10}$ molecules/cm^2 at these surfaces, with associated midpoint redox potentials as expected. Time resolved fluorescence imaging is then carried out with the simultaneous application of a triangular potential wave to the working electrode wherein the fluorescence emission from the surface bound protein adlayers is found to be modulated (being typically some 40–60% higher at potentials cathodic of the midpoint potential). The frequency of fluorescence modulation tracks that of the applied potential sweep rate 180° out of phase (potential wave minima coinciding with fluorescence maxima) as shown in Fig. 8a. Control experiments with either the dye alone or dye labelled non redox active Zn forms of the protein show negligible or minimal fluorescence modulation with surface potential.

Not only does such imaging enable a direct access to surface homogeneity, molecular aggregation (through standard emission imaging) and the degree of redox site coupling to the underlying electrode surface (proteins which are not communicating with the supporting electrode do not optically switch with potential), in tracking surface emission while cycling potential a fluorescence-detected cyclic voltammogram (FCV) can be generated from which midpoint potentials can be directly resolved using modified Butler–Volmer method [133] (Fig. 8b). In addition to the rigorous mathematical treatment within this form of analysis, we have recently demonstrated that such FCV's can be equivalently and more rapidly analyzed by a fully graphical method [134]. It is worth noting that, unlike classical voltammograms where current signal decreases on either side of midpoint potential, FCV's achieve a steady state at asymptotic values (fluorophores that are in specific switch state remain fixed at over potential) resulting in sigmoidal behaviour. Utilizing the fact that fluorescence light intensity reflects the number of azurin molecules in reduced form, we have defined 'optical peak potential' (E_p) as the potential at which rate of change of fluorescent intensity is maximum; which is determined by fitting the FCV plot with Boltzmann sigmoidal equation (Eq. (1)).

$$I_f = I_{f\,min} + \frac{I_{f\,max} - I_{f\,min}}{1 + \exp(E - E_p)/dE} \quad (1)$$

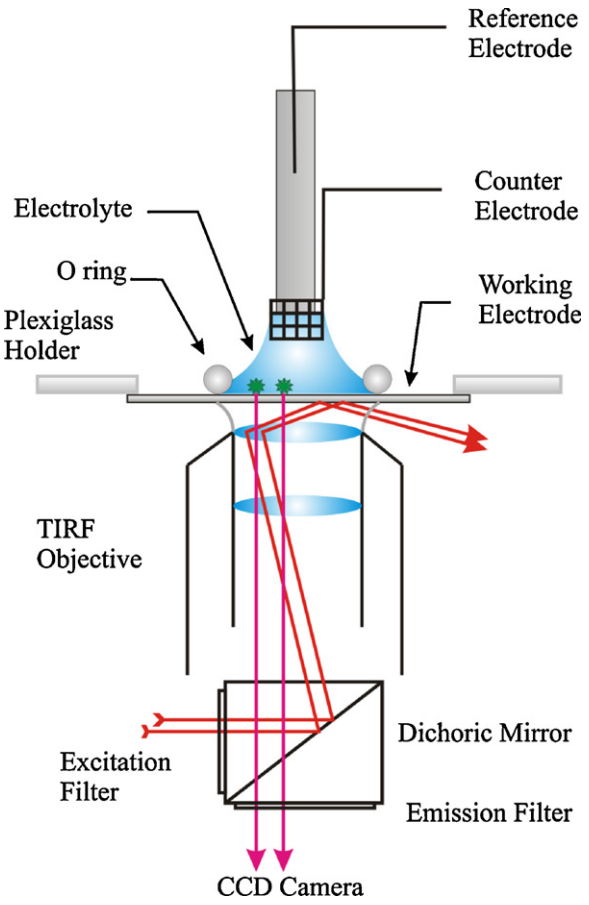

Fig. 7. Schematic representation of a composite electrochemical-TIRF configuration. A home-made single compartment electrochemical cell with a transparent gold working electrode is fixed above TIRF objective of a Nikon TE200-E fluorescence microscope. The excitation source (a 633 nm laser) is filtered and totally internally reflected causing an evanescent wave which excites fluorophore tagged protein. The resulting emission is monitored while the potential of the working electrode is cycled with an externally associated potentiostat (not shown). Reproduced with permission from Ref. [134].

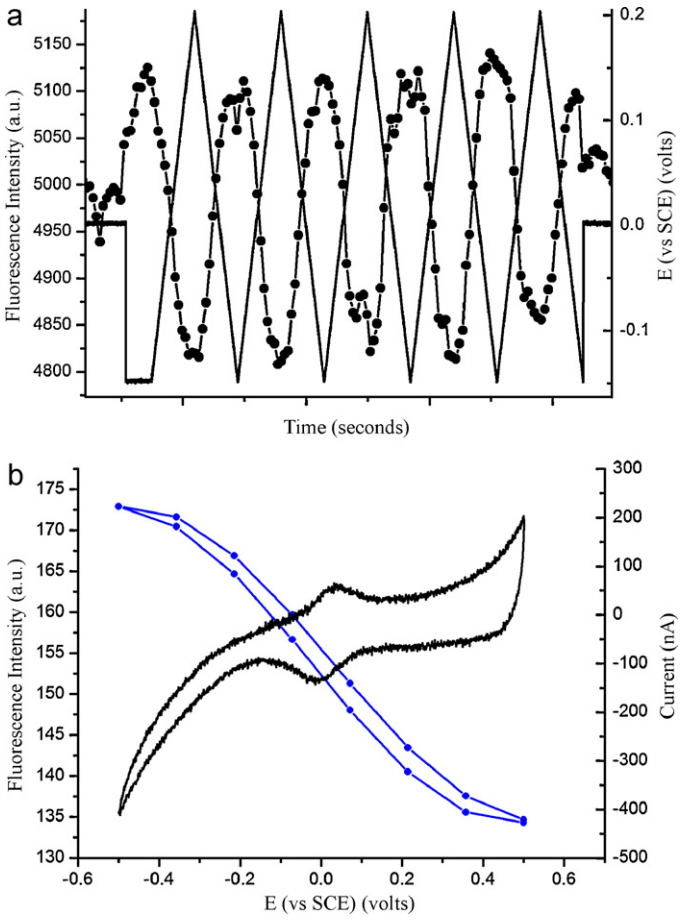

Fig. 8. (a) Time trace plots of applied potential wave (black line) scanned between 0.2 and −0.2 V at a scan rate 200 mV/s overlaid over the resulting (simultaneously acquired) trace of fluorescence intensity (line with black circles). Data acquired here for Atto 655 labelled azurin on an octanethiol modified gold electrode, in phosphate buffer (pH 7.1, 200 mM), using a 633 nm CW laser excitation. Time axis: 5 s per division. (b) CV (black) and FCV (blue line with circles) of Cy5 labelled wt azurin at a scan rate of 100 mV/s. Note the characteristic wave shapes and coincidence of optically determined mid point and electrochemically determined half wave potentials.

By finding the midpoint of averaged optical peak potentials for forward and backward traces, an "Optical Midpoint Potential" (OMP) can be defined.

The amount of redox active protein present within any one diffraction limited spot (the smallest surface element from which optical data are attainable; ~300 nm) is controllable through dilution of the protein solution and the time duration for which the surface is exposed to (submicromolar) protein solutions. At progressively lower surface coverage the faradaic current drops below that which is reliably detectable by standard voltammetric measurements, though optical data acquisition remains relatively trivial. At low submonolayer coverages each (electrochemically) assayed spot can contain as few as a few tens of fluorophore labelled metalloproteins [133]. Such an ability to spatially probe and map interfacial redox events is, we believe, without precedent and immediately highlights dispersion in molecular redox characteristics as shown in Figs. 9 and 10.

The midpoint potential variance observed in such analyses is both significant (up to several tens of millivolts) and observed to be a function of the protein surface density; high surface coverage samples showing a smaller spread (~14 mV within this azurin case study) compared with low submonolayer surfaces (for which the spread is some 70 mV; Fig. 10). The differing spread in midpoint potential across any one form of surface modification is broadly the same within 10% across any one form of surface modification and

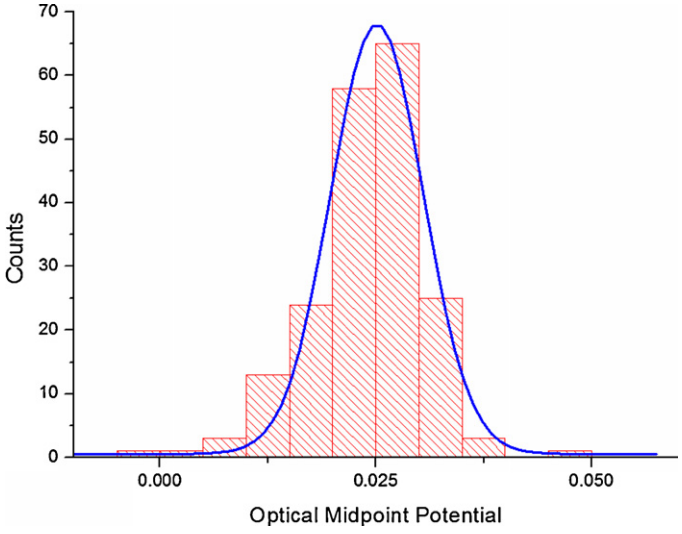

Fig. 9. Gaussian fit to the optically determined midpoint potentials of approximately 6×10^{12} molecules on a decanethiol modified optically transparent gold electrode at an applied scan rate of 200 mV/s. The Gaussian is centred on 25.16 mV (with fwhm of 12.6 mV), which is within 3 mV of the electrochemically determined bulk midpoint potential (surface coverage of 1.5×10^{12} molecules/cm^2). Reprinted with permission from Ref. [134].

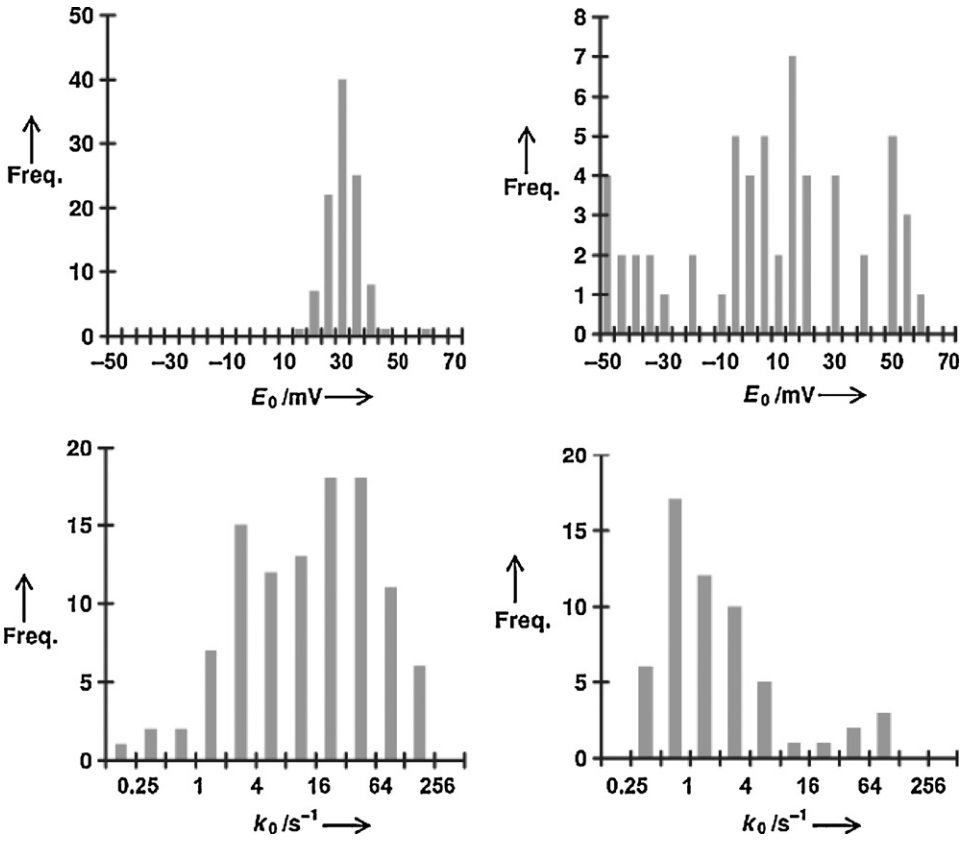

Fig. 10. (a) Histogram of midpoint potential values as obtained with Butler Volmer analysis for a high coverage sample of fluorophore tagged azurin showing 14 mV fwhm spread. (b) Equivalent histogram for a low surface coverage sample showing a much larger spread of 70 mV. (c) Histogram of standard electron transfer rate constants k_0 obtained for high coverage sample with values ranging from 0.1 to 200 s^{-1}. (d) Histogram of standard electron transfer rate constants k_0 for low coverage sample showing values clustered between 0.5 and 2 s^{-1} with a high tail at 100 s^{-1}. Reprinted with permission from Ref. [133].

protein density and will be reflective of both inherent molecular differences (such as the protein fold, for example) and microenvironmental factors such as local fluctuations in the field drop [135,136] and variant discontinuities/imperfections in underlying SAM and/or gold electrode (see below). Significantly, in analysing large amount of such data, it is evident that this dispersion consistently contracts towards a narrower distribution centred close to the bulk determined midpoint potential at higher molecular densities or through more data averaging.

FCV plots show an increase in separation between the oxidizing and reducing curves with increasing voltage sweep rate, a behaviour similar to peak separation in cyclic voltammetry (CV) experiments, and scrutinizable with "standard" kinetic analysis methods [133]. Pleasingly, such analyses show good agreement between FCV and CV (standard electron transfer rate constant k_0: FCV 21 s^{-1}, CV 67 s^{-1} for azurin immobilized on a hexanethiol SAM) with the observed difference potentially ascribable to the relative bias of FCV data towards proteins that are weakly coupled to the electrode surface and thus less quenched by the continuum of gold. As with midpoint potentials, k_0 distributions show a significant spread across any given surface with a notable dependence upon protein surface coverage values (high coverage samples, from which data are averaged, show a more symmetrical distribution in rates; data acquired at sub monolayer coverages are appreciably more scattered; Fig. 10).

Of all the potential microenvironmental parameters that may contribute to a spread in electron transfer characteristics across any given electrode surface the degree of crystallinity within the SAM layer buffering the protein from the metallic electrode surface is experimentally most isolatable and deliberately tuneable. As a single parameter it will, of course, potentially impact a range of contributors including protein surface orientation, solvation, electric field drop (the driving force "seen" by the redox site) and redox-site-electrode electronic coupling. The spontaneous formation of ordered alkanethiol SAMs on gold, due to the strong affinity of sulfur group for gold, has been extensively documented and known to proceed via a sequence of several structural phase transition resulting in monolayer films with hexagonal $(\sqrt{3} \times \sqrt{3})$R30° symmetry (on Au (1 1 1)) [137–140]. Long chain alkanethiols display an additional modulation of $(\sqrt{3} \times \sqrt{3})$ structure, yielding a $c(4 \times 2)$ superlattice with the same molecular concentration and have an associated tilt angle of ~30° to surface normal[141–144]. A range of characterization techniques (ellipsometric, FT-IRRAS and electrochemical) have reported a progress towards lower packing order and density with decreasing chain length, with sharpest transition occurring between C_6 and C_{12} films [141]. This trend line (of increasing order with increasing alkyl chain length) is confirmable on polycrystalline gold electrodes using electrodesorption studies (a cathodic progression of stripping potential with increasing alkyl chain length), contact angle measurements and electrochemical redox probe (to probe structural defects).

In order to probe our ability to chemical tune the degree of order at a biomolecular interface, we have carried out a systematic survey in which FCV data acquired from fluorophore labelled azurin immobilized on a range of alkanethiol (from hexanethiol to dodecanethiol) modified gold electrodes have been analyzed graphically [134]. In carrying out equivalent analyses of multiple ROI's at different locations across a range of identically prepared samples (wherein random variations in experimental conditions such as gold surface variance, localized SAM defects, etc, aver-

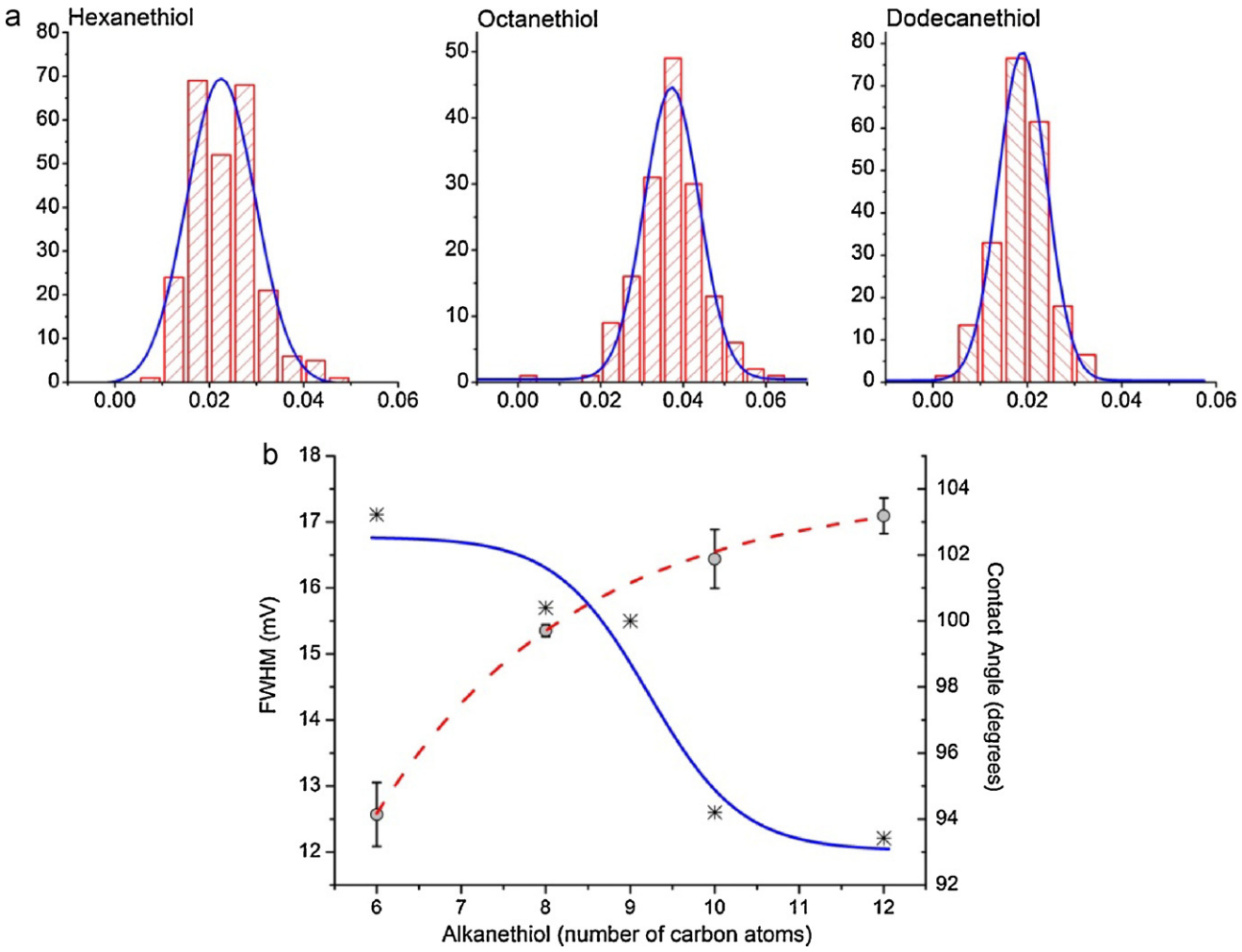

Fig. 11. (a) Comparison of Gaussian fits to optically determined midpoint potentials for wild type azurin tagged with Atto 665 on Hexanethiol (fwhm = 17.11 mV), octanethiol (fwhm = 15.64 mV) and dodecanethiol (fwhm = 12.15 mV), showing a decrease of approximately of 30% in fwhm with increasing chain length. (b) each data point (black star) represents fwhm of a Gaussian fit to an OMP histogram. Each OMP histogram was generated by analysing at least 200 random locations on each sample. The sigmoidal trend (blue line) of decrease in the fwhm with increasing chain length nicely complements the increasing hydrophobicity of alkanethiol monolayer with increasing chain length. Reprinted with permission from Ref. [134].

age out) across a range of supporting alkanethiol monolayers, the spread of midpoint potentials shows a highly reproducible trend. It is, specifically, observed that this dispersion contracts as layers become more crystalline and defect free (Fig. 11) with OMP's typically spanning some 30% greater range with short (hexanethiol) thiol layers than with longer (dodecanethiol).

4. Conclusions

Over the past three decades our ability to controllably interface biomolecules with electrodes and, in some cases, to productively use this communication in the generation of derived sensors, has changed profoundly. For a number of practical reasons, work in this area has progressively evolved from the modification of electrodes in order to facilitate diffusive communication to the controlled and oriented immobilization of proteins and enzymes (and their engineered forms) at the electrode surface ideally such that biological fold and function are retained while electronic coupling to the supporting electrode is maximised. Non-covalent approaches include physical adsorption, entrapment in gels or polymers, hydrophobic, hydrophilic and electrostatic interactions. Covalent methods of immobilization can be site specific through either a single naturally expressed or artificially induced functional group on the protein surface. Protocols for increasing surface loading and electronic coupling using carbon nanotubes and nanoparticles have also been developed. Though conceptually simpler, surface confined bioelectrochemical analyses has almost always generated electrochemical responses which deviate from the ideal (theoretical) behaviour and suffer from experiment to experiment (or lab to lab) variations commonly attributed to the variant contributions from electrode surface mechanical and electronic inhomogeneity, dispersion in molecular orientation, lateral interactions between redox sites, supporting monolayer variations. These contributions are, however, rarely quantified or assigned with the support of experimental data.

As with all "bulk" analyses, the faradaic responses obtained in these experiments are reflective of the average behaviour of all molecules being sampled – this is typically 10^{12}–10^{14} molecules in a bioelectrochemical experiment (depending upon electrode area and surface coverage). The result is that an average distribution of properties is recorded and, as such, there is an increasing disparity between the functional "redox data" and the capabilities of state of the art imaging equipment (which can topographically resolve individual molecules). As interest in the generation of derived "nano-bio devices", composed of low numbers of biomolecules, grows, a detailed knowledge of molecular dispersion becomes not only fundamentally interesting but also fundamentally important. Though distributions in surface bio-redox properties have been

referred to or indeed assumed for some time, and a significant part of the "non-idealities" reported are likely to be ascribable to directly associated non-idealities within the film structure, the methods by which this can be directly resolved are limited. We have sought, then, to both utilize near field tunnelling and far field FRET coupled imaging configurations to directly analyze the electron transfer characteristics of surface immobilized biomolecules at molecular scales. By combining the imaging resolution of an STM or CPAFM with electrochemical potential control, it is, specifically, possible to obtain high resolution conductance images of electrode-confined protein molecules and to carry out functional mapping based on current/voltage and conductance-surface potential relationships. Observations possible within such experimental formats generate a wealth of information about surface homogeneity, molecular conductance, redox site coupling to supporting electrodes and switching potentials at truly molecular scales.

The optical characteristics of redox active centres can also be utilized in enabling a direct imaging of electron transfer. We have specifically made use of the large modulation in ligand-to-metal-charge transfer associated with blue copper proteins as a function of their redox state. In coupling these changes to the FRET based communication with an externally appended fluorophore, the redox state of these proteins can be directly imaged by means of far field fluorescence. At suitable levels of dilution, on optically transparent electrode surfaces, reversible interfacial electron transfer processes can be followed pixel by pixel down to scales which approach the molecular. One can define from such imaging the midpoint potentials of these molecules and, significantly, map this out across a surface population, empowering a direct, quantified and highly reproducible resolution of thermodynamic dispersion. The self assembled monolayer buffering the protein from the underlying metallic electrode surface in these (and many similar) studies acts not only to tune electronic coupling between the two but also potentially provides a variable more easily segmented from other contributions to molecular dispersion. We have, specifically, considered the possibility that the supporting monolayer crystallinity be a significant contributor to the subsequently observed spread in midpoint potentials and indeed this is certainly the case for the blue copper protein azurin (this spread diminishes from 17 mV to 12 mV as the supporting alkanethiol layer crystallinity increases). An extrapolation of this methodology to a range of redox active proteins and enzymes is, in many cases, obvious.

This potential importance and application of interfacial bioelectronics remains substantial; much can be achieved through a combination of surface and biological engineering. This article has sought to highlight some of the capabilities afforded by imaging technologies in not only enabling a direct molecular level resolution of such interfaces but also a highly spatially resolved mapping of their functionality.

Acknowledgements

The authors acknowledge financial support from the Engineering and Physical Sciences Research Council (UK; Grant GR/S71811/01), The Leverhulme Trust (UK; Grant F/699/D), and the EU (EdRox Program). They also acknowledge the contributions made to this work by collaborating teams in the departments of Chemistry and Physics at the University of Leiden, Holland, most notably those of Professor's Thijs Aartsma and Professor Gerard Canters.

References

[1] P. Yeh, T. Kuwana, Chem. Lett. 6 (1977) 1145.
[2] M.J. Eddowes, H.A.O. Hill, J. Chem. Soc.-Chem. Commun. (1977) 771.
[3] Q. Chi, J. Zhang, J.E.T. Andersen, J. Ulstrup, J. Phys. Chem. B 105 (2001) 4669.
[4] I. Gill, Chem. Mater. 13 (2001) 3404.
[5] K.J. McKenzie, F. Marken, Langmuir 19 (2003) 4327.
[6] Y. Zhang, P.L. He, N.F. Hu, Electrochim. Acta 49 (2004) 1981.
[7] S.J. Guo, S.J. Dong, Trac-Trends Anal. Chem. 28 (2009) 96.
[8] L.M. Ellerby, R.N. Clinton, F. Nishida, S.A. Yamanaka, B. Dunn, J.S. Valentine, J.I. Zink, Science 255 (1992) 1113.
[9] B.C. Dave, B. Dunn, J.S. Valentine, J.I. Zink, Anal. Chem. 66 (1994) 1120A.
[10] Q. Ji, C.R. Lloyd, W.R. Ellis, E.M. Eyring, J. Am. Chem. Soc. 120 (1998) 221.
[11] T.K. Das, I. Khan, D.L. Rousseau, J.M. Friedman, J. Am. Chem. Soc. 120 (1998) 10268.
[12] Q.L. Wang, G.X. Lu, B.J. Yang, Langmuir 20 (2004) 1342.
[13] D. Deriu, S.E. Pagnotta, R. Santucci, N. Rosato, Biometals 21 (2008) 417.
[14] S. Cosnier, Anal. Bioanal. Chem. 377 (2003) 507.
[15] J.J. Davis, R.J. Coles, H.A.O. Hill, J. Electroanal. Chem. 440 (1997) 279.
[16] S.C. Tsang, J.J. Davis, M.L.H. Green, H.A.O. Hill, Y.C. Leung, P.J. Sadler, J. Chem. Soc., Chem. Commun. (1995) 1803.
[17] J.J. Davis, M.L.H. Green, H. Allen, O. Hill, Y.C. Leung, P.J. Sadler, J. Sloan, A.V. Xavier, S. Chi Tsang, Inorg. Chim. Acta 272 (1998) 261.
[18] G. Wang, J.-J. Xu, H.-Y. Chen, Electrochem. Commun. 4 (2002) 506.
[19] G.-C. Zhao, L. Zhang, X.-W. Wei, Z.-S. Yang, Electrochem. Commun. 5 (2003) 825.
[20] J. Wang, M. Li, Z. Shi, N. Li, Z. Gu, Anal. Chem. 74 (2002) 1993.
[21] J. Wang, Electroanalysis 17 (2005) 7.
[22] X. Yu, D. Chattopadhyay, I. Galeska, F. Papadimitrakopoulos, J.F. Rusling, Electrochem. Commun. 5 (2003) 408.
[23] X. Yu, B. Munge, V. Patel, G. Jensen, A. Bhirde, J.D. Gong, S.N. Kim, J. Gillespie, J.S. Gutkind, F. Papadimitrakopoulos, J.F. Rusling, J. Am. Chem. Soc. 128 (2006) 11199.
[24] B.V. Chikkaveeraiah, A. Bhirde, R. Malhotra, V. Patel, J.S. Gutkind, J.F. Rusling, Anal. Chem. 81 (2009) 9129.
[25] K.R. Brown, A.P. Fox, M.J. Natan, J. Am. Chem. Soc. 118 (1996) 1154.
[26] S. Liu, D.n. Leech, H. Ju, Anal. Lett. 36 (2003) 1.
[27] E. Topoglidis, C.J. Campbell, A.E.G. Cass, J.R. Durrant, Langmuir 17 (2001) 7899.
[28] Q. Li, G. Luo, J. Feng, Electroanalysis 13 (2001) 359.
[29] K.R. Meier, M. Grätzel, Chem. Phys. Chem. 3 (2002) 371.
[30] Y. Lvov, B. Munge, O. Giraldo, I. Ichinose, S.L. Suib, J.F. Rusling, Langmuir 16 (2000) 8850.
[31] Q. Gao, S.L. Suib, J.F. Rusling, Chem. Commun. (2002) 2254.
[32] D.H.P. Hedges, D.J. Richardson, D.A. Russell, Langmuir 20 (2004) 1901.
[33] A. El Kasmi, M.C. Leopold, R. Galligan, R.T. Robertson, S.S. Saavedra, K. El Kacemi, E.F. Bowden, Electrochem. Commun. 4 (2002) 177.
[34] S. Ciampi, J.J. Gooding, Chem. -Eur. J. 16 (2010) 5961.
[35] C. Mu, Q. Zhao, D.S. Xu, Q.K. Zhuang, Y.H. Shao, J. Phys. Chem. B 111 (2007) 1491.
[36] A. Hartl, E. Schmich, J.A. Garrido, J. Hernando, S.C.R. Catharino, S. Walter, P. Feulner, A. Kromka, D. Steinmuller, M. Stutzmann, Nat. Mater. 3 (2004) 736.
[37] F.A. Armstrong, H.A.O. Hill, B.N. Oliver, N.J. Walton, J. Am. Chem. Soc. 106 (1984) 921.
[38] F.A. Armstrong, P.A. Cox, H.A.O. Hill, V.J. Lowe, B.N. Oliver, J. Electroanal. Chem. 217 (1987) 331.
[39] J. Hirst, F.A. Armstrong, Anal. Chem. 70 (1998) 5062.
[40] F.A. Armstrong, R. Camba, H.A. Heering, J. Hirst, L.J.C. Jeuken, A.K. Jones, C. Leger, J.P. McEvoy, Faraday Discuss. 116 (2000).
[41] C.F. Blanford, F.A. Armstrong, J. Solid State Electrochem. 10 (2006) 826.
[42] N.K. Chaki, K. Vijayamohanan, Biosens. Bioelectron. 17 (2002) 1.
[43] S. Song, R.A. Clark, E.F. Bowden, J. Phys. Chem. 97 (1993) 6564.
[44] T.M. Nahir, E.F. Bowden, J. Electroanal. Chem. 410 (1996) 9.
[45] A. Avila, B.W. Gregory, K. Niki, T.M. Cotton, J. Phys. Chem. B 104 (2000) 2759.
[46] M.J. Tarlov, E.F. Bowden, J. Am. Chem. Soc. 113 (1991) 1847.
[47] M. Collinson, E.F. Bowden, M.J. Tarlov, Langmuir 8 (1992) 1247.
[48] O. Farver, Y. Blatt, I. Pecht, Biochemistry 21 (1982) 3556.
[49] M. Van de Kamp, R. Floris, F.C. Hali, G.W. Canters, J. Am. Chem. Soc. 112 (1990) 907.
[50] M. van de Kamp, M.C. Silvestrini, M. Brunori, J. Van Beeumen, F.C. Hali, G.W. Canters, Eur. J. Biochem. 194 (1990) 109.
[51] A.K. Gaigalas, G. Niaura, J. Colloid Interface Sci. 193 (1997) 60.
[52] Q. Chi, J. Zhang, P.S. Jensen, H.E.M. Christensen, J. Ulstrup, Faraday Discuss. 131 (2006) 181.
[53] J.J. Davis, B. Peters, W. Xi, J. Appel, A. Kros, T.J. Aartsma, R. Stan, G.W. Canters, J. Phys. Chem. Lett. 1 (2010) 1541.
[54] L. Andolfi, D. Bruce, S. Cannistraro, G.W. Canters, J.J. Davis, H.A.O. Hill, J. Crozier, M.P. Verbeet, C.L. Wrathmell, Y. Astier, J. Electroanal. Chem. 565 (2004) 21.
[55] O. Cavalleri, C. Natale, M.E. Stroppolo, A. Relini, E. Cosulich, S. Thea, M. Novi, A. Gliozzi, Phys. Chem. Chem. Phys. 2 (2000) 4630.
[56] P. Fristrup, M. Grubb, J. Zhang, H.E.M. Christensen, A.M. Hansen, J. Ulstrup, J. Electroanal. Chem. 511 (2001) 128.
[57] J. Davis, D.A. Morgan, C.L. Wrathmell, D.N. Axford, J. Zhao, N. Wang, J. Mater. Chem. 15 (2005) 2160.
[58] M.L. Vargo, C.P. Gulka, J.K. Gerig, C.M. Manieri, J.D. Dattelbaum, C.B. Marks, N.T. Lawrence, M.L. Trawick, M.C. Leopold, Langmuir 26 (2009) 560.
[59] D.E. Khoshtariya, T.D. Dolidze, M. Shushanyan, K.L. Davis, D.H. Waldeck, R. van Eldik, Proc. Natl. Acad. Sci. U.S.A. 107 (2010) 2757.
[60] J.J. Davis, C.M. Halliwell, H.A.O. Hill, G.W. Canters, M.C. van Amsterdam, M.Ph. Verbeet, New J. Chem. 22 (1998).
[61] J.J. Davis, D. Djuricic, K.K.W. Lo, E.N.K. Wallace, L.-L. Wong, H.A.O. Hill, Faraday Discuss. 116 (2000) 15.

[62] A. Fantuzzi, S. Sadeghi, F. Valetti, G.L. Rossi, G. Gilardi, Biochemistry 41 (2002) 8718.
[63] A. Fantuzzi, M. Fairhead, G. Gilardi, J. Am. Chem. Soc. 126 (2004) 5040.
[64] V.E.V. Ferrero, L. Andolfi, G. Di Nardo, S.J. Sadeghi, A. Fantuzzi, S. Cannistraro, G. Gilardi, Anal. Chem. 80 (2008) 8438.
[65] J.J. Davis, H.A.O. Hill, A.M. Bond, Coord. Chem. Rev. 200–202 (2000) 411.
[66] J. Davis, H.A.O. Hill, Chem. Commun. (2002) 393.
[67] J.J. Davis, D. Bruce, G.W. Canters, J. Crozier, H.A.O. Hill, Chem. Commun. (2003) 576.
[68] J. Zhao, J.J. Davis, M.S.P. Sansom, A. Hung, J. Am. Chem. Soc. 126 (2004) 5601.
[69] C.P. Smith, H.S. White, Anal. Chem. 64 (1992) 2398.
[70] M.J. Honeychurch, G.A. Rechnitz, Electroanalysis 10 (1998) 285.
[71] R.A. Clark, E.F. Bowden, Langmuir 13 (1997) 559.
[72] J. Petrovic, R.A. Clark, H. Yue, D.H. Waldeck, E.F. Bowden, Langmuir 21 (2005) 6308.
[73] R.E. Palacios, F.-R.F. Fan, A.J. Bard, P.F. Barbara, J. Am. Chem. Soc. 128 (2006) 9028.
[74] R.E. Palacios, F.-R.F. Fan, J.K. Grey, J. Suk, A.J. Bard, P.F. Barbara, Nat. Mater. 6 (2007) 680.
[75] F.-R.F. Fan, A.J. Bard, Science 267 (1995) 871.
[76] A.J. Bard, F.-R.F. Fan, Acc. Chem. Res. 29 (1996) 572.
[77] F.J.M. Hoeben, F.S. Meijer, C. Dekker, S.P.J. Albracht, H.A. Heering, S.G. Lemay, ACS Nano (2008).
[78] H.A. Heering, F.G.M. Wiertz, C. Dekker, S. de Vries, J. Am. Chem. Soc. 126 (2004) 11103.
[79] M. Rief, F. Oesterhelt, B. Heymann, H.E. Gaub, Science 275 (1997) 1295.
[80] F. Oesterhelt, D. Oesterhelt, M. Pfeiffer, A. Engel, H.E. Gaub, D.J. Muller, Science 288 (2000) 143.
[81] A. Engel, D.J. Muller, Nat. Struct. Biol. 7 (2000) 715.
[82] M. Carrion-Vazquez, A.F. Oberhauser, T.E. Fisher, P.E. Marszalek, H.B. Li, J.M. Fernandez, Prog. Biophys. Mol. Biol. 74 (2000) 63.
[83] H.G. Hansma, Annu. Rev. Phys. Chem. 52 (2001) 71.
[84] D. Fotiadis, S. Scheuring, S.A. Muller, A. Engel, D.J. Muller, Micron 33 (2002) 385.
[85] H.F. Knapp, P. Mesquida, A. Stemmer, Surf. Interface Anal. 33 (2002) 108.
[86] D. Fotiadis, Y. Liang, S. Filipek, D.A. Saperstein, A. Engel, K. Palczewski, Nature 421 (2003) 127.
[87] D.P. Allison, N.P. Mortensen, C.J. Sullivan, M.J. Doktycz, Wiley Interdiscip. Rev. -Nanomed. Nanobiotechnol. 2 (2010) 618.
[88] J. Hu, Y. Zhang, H.B. Gao, M.Q. Li, U. Hartmann, Nano Lett. 2 (2002) 55.
[89] F.J. Rubio-Sierra, W.M. Heckl, R.W. Stark, Adv. Eng. Mater. 7 (2005) 193.
[90] H. Seelert, A. Poetsch, N.A. Dencher, A. Engel, H. Stahlberg, D.J. Muller, Nature 405 (2000) 418.
[91] D.J. Müller, H.-J. Sass, S.A. Müller, G. Büldt, A. Engel, J. Mol. Biol. 285 (1999) 1903.
[92] H.G. Hansma, D.E. Laney, M. Bezanilla, R.L. Sinsheimer, P.K. Hansma, Biophys. J. 68 (1995) 1672.
[93] C. Möller, M. Allen, V. Elings, A. Engel, D.J. Müller, Biophys. J. 77 (1999) 1150.
[94] S.N. Magonov, V. Elings, M.H. Whangbo, Surf. Sci. 375 (1997) L385.
[95] M.-H. Whangbo, G. Bar, R. Brandsch, Surf. Sci. 411 (1998) L794.
[96] C.D. Frisbie, L.F. Rozsnyai, A. Noy, M.S. Wrighton, C.M. Lieber, Science 265 (1994) 2071.
[97] R. McKendry, M.-E. Theoclitou, T. Rayment, C. Abell, Nature 391 (1998) 566.
[98] D.C. Cullen, C.R. Lowe, J. Colloid Interface Sci. 166 (1994) 102.
[99] M. Quinto, A. Ciancio, P.G. Zambonin, J. Electroanal. Chem. 448 (1998) 51.
[100] X.Q. Ding, J.B. Hu, Q.L. Li, Talanta 68 (2006) 653.
[101] K. Nakano, T. Yoshitake, Y. Yamashita, E.F. Bowden, Langmuir 23 (2007) 6270.
[102] K.G. Arzola, Y. Gimeno, M.C. Arevalo, M.A. Falcon, A.H. Creus, Bioelectrochemistry 79 (2010) 17.
[103] F. Ogletree, M. Salmeron, Prog. Solid State Chem. 20 (1990) 235.
[104] J.K. Gimzewski, C. Joachim, Science 283 (1999) 1683.
[105] F. Rosei, M. Schunack, Y. Naitoh, P. Jiang, A. Gourdon, E. Laegsgaard, I. Stensgaard, C. Joachim, F. Besenbacher, Prog. Surf. Sci. 71 (2003) 95.
[106] E.P. Friis, Y.I. Kharkats, A.M. Kuznetsov, J. Ulstrup, J. Phys. Chem. A 102 (1998) 7851.
[107] Z. Nawaz, T.R.I. Cataldi, J. Knall, R. Somekh, J.B. Pethica, Surf. Sci. 265 (1992) 139.
[108] S. Boussaad, N.J. Tao, R. Arechabaleta, Chem. Phys. Lett. 280 (1997) 397.
[109] P.B. Lukins, T. Oates, Biochimica et Biophysica Acta (BBA) – Bioenergetics 1409 (1998) 1.
[110] D. Hobara, S.-i. Imabayashi, T. Kakiuchi, Nano Lett. 2 (2002) 1021.
[111] B. Bonanni, D. Alliata, A.R. Bizzarri, S. Cannistraro, Chem. Phys. Chem. 4 (2003) 1183.
[112] A.R. Bizzarri, L. Andolfi, M. Stchakovsky, S. Cannistraro, AZojono 1 (2005).
[113] L. Andolfi, B. Bonanni, G.W. Canters, M.P. Verbeet, S. Cannistraro, Surf. Sci. 530 (2003) 181.
[114] J. Zhao, J. Davis, Nanotechnology 14 (2003) 1023.
[115] J.J. Davis, C.L. Wrathmell, J. Zhao, J. Fletcher, J. Mol. Recognit. 17 (2004) 167.
[116] D. Axford, J.J. Davis, N. Wang, D. Wang, T. Zhang, J. Zhao, B. Peters, J. Phys. Chem. B 111 (2007) 9062.
[117] J.J. Davis, B. Peters, W. Xi, J. Phys.: Condens. Mat. 20 (2008) 374123.
[118] J.J. Davis, N. Wang, A. Morgan, T. Zhang, J. Zhao, Faraday Discuss. 131 (2006) 167.
[119] N.J. Tao, Phys. Rev. Lett. 76 (1996) 4066.
[120] A.M. Kuznetsov, J. Ulstrup, J. Phys. Chem. A 104 (2000) 11531.
[121] P. Facci, D. Alliata, S. Cannistraro, Ultramicroscopy 89 (2001) 291.
[122] J. Zhang, Q. Chi, A.M. Kuznetsov, A.G. Hansen, H. Wackerbarth, H.E.M. Christensen, J.E.T. Andersen, J. Ulstrup, J. Phys. Chem. B 106 (2002) 1131.
[123] W. Haiss, H. van Zalinge, S.J. Higgins, D. Bethell, H. Hobenreich, D.J. Schiffrin, R.J. Nichols, J. Am. Chem. Soc. 125 (2003) 15294.
[124] A.M. Ricci, E.J. Calvo, S. Martin, R.J. Nichols, J. Am. Chem. Soc. 132 (2010) 2494.
[125] E.P. Friis, J.E.T. Andersen, L.L. Madsen, P. Moller, J. Ulstrup, J. Electroanal. Chem. 431 (1997) 35.
[126] J.J. Davis, D.A. Morgan, C.L. Wrathmell, A. Zhao, IEE Proc. Nanobiotechnol. 151 (2004) 37.
[127] Q.J. Chi, J.D. Zhang, P.S. Jensen, H.E.M. Christensen, J. Ulstrup, Faraday Discuss. 131 (2006) 181.
[128] A. Alessandrini, M. Salerno, S. Frabboni, P. Facci, Appl. Phys. Lett. 86 (2005) 133902.
[129] J. Davis, H. Burgess, G. Zauner, S. Kuznetsova, J. Salverda, T. Aartsma, G.W. Canters, J. Phys. Chem. B 110 (2006) 20649.
[130] R. Schmauder, S. Alagaratnam, C. Chan, T. Schmidt, G.W. Canters, T.J. Aartsma, J. Biol. Inorg. Chem. 10 (2005) 683.
[131] R. Schmauder, F. Librizzi, G.W. Canters, T. Schmidt, T. Aartsma, Chem. Phys. Chem. 6 (2005) 1381.
[132] S. Kuznetsova, G. Zauner, R. Schmauder, O.A. Mayboroda, A.M. Deelder, T. Aartsma, G.W. Canters, Anal. Biochem. 350 (2006) 52.
[133] J. Salverda, A. Patil, G. Mizzon, S. Kuznetsova, G. Zauner, N. Akkilic, G. Canters, J. Davis, H. Heering, T. Aartsma, Angew. Chem. Int. Ed. Engl. 122 (2010) 5912.
[134] A.V. Patil, J.J. Davis, J. Am. Chem. Soc. 132 (2010) 16938.
[135] F. Drepper, M. Hippler, W. Nitschke, W. Haehnel, Biochemistry 35 (1996) 1282.
[136] D.H. Murgida, P. Hildebrandt, Chem. Soc. Rev. 37 (2008) 937.
[137] C.D. Bain, G.M. Whitesides, J. Am. Chem. Soc. 110 (1988) 6560.
[138] C.D. Bain, E.B. Troughton, Y.T. Tao, J. Evall, G.M. Whitesides, R.G. Nuzzo, J. Am. Chem. Soc. 111 (1989) 321.
[139] M. Kawasaki, T. Sato, T. Tanaka, K. Takao, Langmuir 16 (2000) 1719.
[140] C. Vericat, M.E. Vela, G.A. Benitez, J.A.M. Gago, X. Torrelles, R.C. Salvarezza, J. Phys.: Condens. Mat. 18 (2006) R867.
[141] M.D. Porter, T.B. Bright, D.L. Allara, C.E.D. Chidsey, J. Am. Chem. Soc. 109 (1987) 3559.
[142] L.H. Dubois, B.R. Zegarski, R.G. Nuzzo, J. Chem. Phys. 98 (1993) 678.
[143] T. Fukuma, K. Kobayashi, T. Horiuchi, H. Yamada, K. Matsushige, Appl. Phys. A 72 (2001) S109.
[144] M. Godin, P.J. Williams, V. Tabard-Cossa, O. Laroche, L.Y. Beaulieu, R.B. Lennox, P. Gruetter, Langmuir 20 (2004) 7090.
[145] E.T. Adman, L.H. Jensen, Israel J. Chem. 21 (1981) 8.